

# Anomalous Shape Evolution of $\text{Ag}_2\text{O}_2$ Nanocrystals Modulated by Surface Adsorbates during Electron Beam Etching

Qiubo Zhang,<sup>†,‡</sup> Guoping Gao,<sup>‡</sup> Yuting Shen,<sup>†,⊥</sup> Xinxing Peng,<sup>‡</sup> Junyi Shangguan,<sup>‡</sup> Yu Wang,<sup>‡</sup> Hui Dong,<sup>†</sup> Karen Bustillo,<sup>§</sup> Linwang Wang,<sup>‡</sup> Litao Sun,<sup>\*,†,⊕</sup> and Haimei Zheng<sup>\*,‡,||,⊕</sup>

<sup>†</sup>SEU-FEI Nano-Pico Center, Key Laboratory of MEMS of Ministry of Education, Collaborative Innovation Center for Micro/Nano Fabrication, Device and System, Southeast University, Nanjing 210018, People's Republic of China

<sup>‡</sup>Materials Science Division, Lawrence Berkeley National Laboratory, Berkeley, California 94720, United States

<sup>⊥</sup>College of Physics and Electronic Engineering, Changshu Institute of Technology, Changshu 215500, People's Republic of China

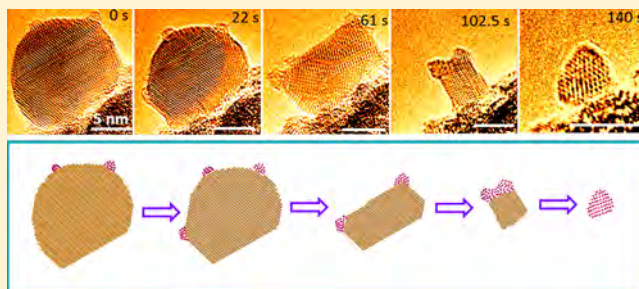
<sup>§</sup>National Center for Electron Microscopy, Molecular Foundry, Lawrence Berkeley National Laboratory, Berkeley, California 94720, United States

<sup>||</sup>Department of Materials Science and Engineering, University of California, Berkeley, Berkeley, California 94720, United States

## Supporting Information

**ABSTRACT:** An understanding of nanocrystal shape evolution is significant for the design, synthesis, and applications of nanocrystals with surface-enhanced properties such as catalysis or plasmonics. Surface adsorbates that are selectively attached to certain facets may strongly affect the atomic pathways of nanocrystal shape development. However, it is a great challenge to directly observe such dynamic processes in situ with a high spatial resolution. Here, we report the anomalous shape evolution of  $\text{Ag}_2\text{O}_2$  nanocrystals modulated by the surface adsorbates of Ag clusters during electron beam etching, which is revealed through in situ transmission electron microscopy (TEM). In contrast to the  $\text{Ag}_2\text{O}_2$  nanocrystals without adsorbates, which display the near-equilibrium shape throughout the etching process,  $\text{Ag}_2\text{O}_2$  nanocrystals with Ag surface adsorbates show distinct facet development during etching by electron beam irradiation. Three stages of shape changes are observed: a sphere-to-a cube transformation, side etching of a cuboid, and bottom etching underneath the surface adsorbates. We find that the Ag adsorbates modify the  $\text{Ag}_2\text{O}_2$  nanocrystal surface configuration by selectively capping the junction between two neighboring facets. They prevent the edge atoms from being etched away and block the diffusion path of surface atoms. Our findings provide critical insights into the modulatory function of surface adsorbates on the shape control of nanocrystals.

**KEYWORDS:** *In situ TEM, shape evolution, surface adsorbates,  $\text{Ag}_2\text{O}_2$  nanocrystal, electron beam etching*



Shape control of nanocrystals has been a significant topic since it directly impacts the physical and chemical properties of nanocrystals in catalysis,<sup>1,2</sup> photonics,<sup>3,4</sup> energy conversion,<sup>5–7</sup> and other applications.<sup>8–11</sup> For a nanocrystal, the equilibrium shape evolution can be predicted by the Wulff construction theory, where the rate of each individual facet change is dependent on the different surface facet energy.<sup>12–14</sup> However, the nanocrystal surface energy can be modified by introducing surfactants, polymeric molecules, or other adsorbates on the nanocrystal surface.<sup>15</sup> These surface agents affect the relative rate changes of different facets through selective capping or providing preferential atomic paths of shape evolution.<sup>15</sup>

Small adsorbates with a strong stability can alter the energy and reactivity of a crystal surface by forming a “capping” layer,<sup>16</sup> which has been considered as a new class of effective shape controllers for nanocrystals.<sup>15</sup> For instance, it was revealed that  $\text{Ag}^+$  ions can promote the formation of (111)

facets of Pt nanocrystals.<sup>15,17</sup> Halides prefer to adsorb on the (100) facets of Pd and Rh to facilitate the formation of Pd and Rh nanocubes.<sup>18,19</sup> Understanding the microscopic mechanisms of surface adsorbates in the shape control of nanocrystals is significant to the functional design and shape control of nanocrystals. In this regard, a great amount of work has been dedicated to the in situ study of the nanocrystal shape evolution.<sup>20,21</sup> For example, we previously investigated the facet development of Pt nanocrystals under the influence of surface ligands during growth.<sup>20,21</sup> Ye et al. studied the nonequilibrium shape evolution of individual gold nanocrystals during oxidative etching.<sup>21</sup> However, how surface adsorbates influence the atomic pathways of nonequilibrium shape

**Received:** November 22, 2018

**Revised:** December 16, 2018

**Published:** December 24, 2018



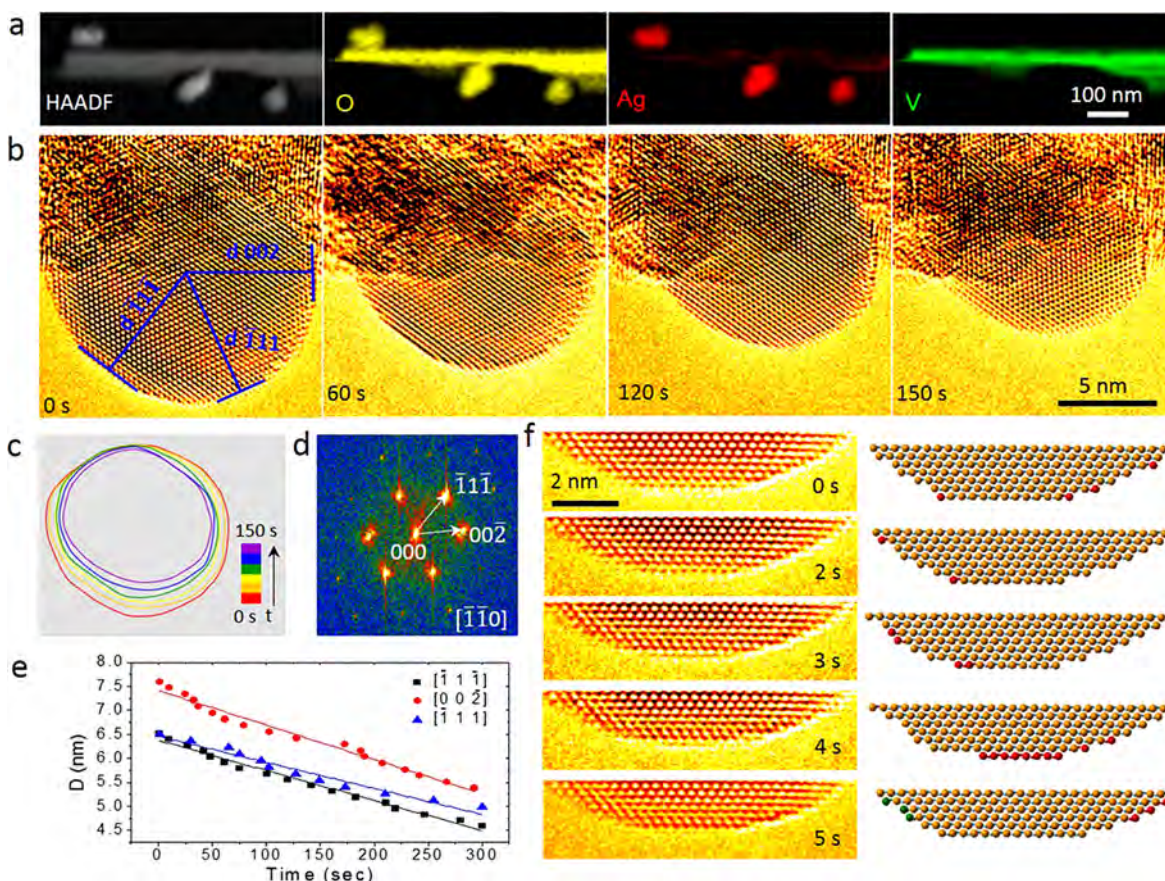


**Figure 1.** Near-equilibrium shape evolution of a  $\text{Ag}_2\text{O}_2$  nanocrystal during electron beam etching. (a) HAADF-STEM image and EELS maps of individual  $\text{AgVO}_3$  nanorods decorated with  $\text{Ag}_2\text{O}_2$  particles. (b) Sequential HRTEM images (false color) show the real-time shape evolution of a  $\text{Ag}_2\text{O}_2$  nanocrystal during electron beam etching. Images are extracted from Video S1. (c) The corresponding time-labeled contours indicate that the sphere-like shape persists during the etching process. (d) The FFT pattern of the  $\text{Ag}_2\text{O}_2$  nanocrystal in part b. (e) The measured average distance from the center of nanocrystal to each facet as a function of time. (f) In situ electron beam etching details of the outermost (111) facet of  $\text{Ag}_2\text{O}_2$ . HRTEM images are listed on the left, and the corresponding stick-and-ball models are displayed on the right. The red balls indicate the atoms to be removed in the next frame, and the green balls indicate the newly appearing adatoms in this frame.

evolution during etching processes is still far from well understood.

Electron beam irradiation has been used to etch materials with nanometric<sup>22–25</sup> or subnanometric<sup>26–28</sup> precision. The etching process can be monitored in the TEM in real time, which allows one to study the impact of surface adsorbates on shape evolution of nanocrystals directly.

Here, we use in situ TEM to study the influences of Ag surface adsorbates on shape evolution of  $\text{Ag}_2\text{O}_2$  nanocrystals during electron beam etching. Since Ag surface adsorbates are much more stable than the  $\text{Ag}_2\text{O}_2$  nanocrystal under electron beam irradiation,<sup>29</sup> the atoms capped by surface adsorbates may be protected from being etched away. The  $\text{Ag}_2\text{O}_2/\text{Ag}$  samples were prepared in situ. First,  $\text{AgVO}_3$  nanorods were synthesized by a hydrothermal method.<sup>30</sup> Then,  $\text{Ag}_2\text{O}_2$  nanocrystals were formed on the surface of  $\text{AgVO}_3$  nanorods using a low flux electron beam and an oxidation treatment (Figure 1a and Figures S1–3). A Cs-corrected TEM (FEI Titan 80–300) operating with an acceleration voltage of 300 kV and with a parallel electron beam (current density  $\sim 2.3 \times 10^6 \text{ A m}^{-2}$ ) was used for the study. The etching of  $\text{Ag}_2\text{O}_2$  nanocrystals was initiated by electron beam irradiation. The entire etching process was captured with atomic resolution and in real time. The results show that the Ag surface adsorbates have a modulatory function, which includes both selective

capping on the surface of  $\text{Ag}_2\text{O}_2$  nanocrystals and blocking of the diffusion path of adatoms. The effects of surface adsorbates should be considered for the fabrication of nanomaterials with different nonequilibrium shapes.

## ■ RESULT AND DISCUSSION

Figure 1 shows that the typical etching of  $\text{Ag}_2\text{O}_2$  nanocrystals without surface adsorbates follows the near-equilibrium shape evolution. The electron energy loss spectra (EELS) maps of  $\text{Ag}_2\text{O}_2$  nanocrystals supported on  $\text{AgVO}_3$  nanorods show that these nanoparticles contain Ag and O elements; the V element only exists in  $\text{AgVO}_3$  nanorods (Figure 1a, Figure S3). High-resolution transmission electron microscope (HRTEM) images (Figure 1b) and the corresponding fast Fourier transform (FFT) pattern show that the crystal structure of  $\text{Ag}_2\text{O}_2$  nanocrystal is monoclinic (Table S1; also see Figure S4 for a more detailed structural characterization). Figure 1b shows the real-time shape evolution of a  $\text{Ag}_2\text{O}_2$  nanocrystal along the  $[\bar{1}10]$  viewing axis during etching. There is no obvious change in the crystal structure while the particle size reduces gradually, and the sphere-like shape is maintained throughout the entire etching process. The original HRTEM images of Figure 1b are shown in Figure S5. To better understand the details of etching, we construct time-labeled contour plots with equal time intervals (Figure 1c). The results

Table 1. Calculated Surface Energy per Ag Atom of Different Crystal Facets

surface energy (eV)	facets						
	{002}	{113}	{200}	$\{\bar{1}11\}$	$\{\bar{1}\bar{1}\bar{1}\}$	$\{\bar{1}\bar{1}\bar{3}\}$	$\{\bar{2}20\}$
	1.98	2.01	2.05	1.57	1.86	2.32	2.40
							2.23

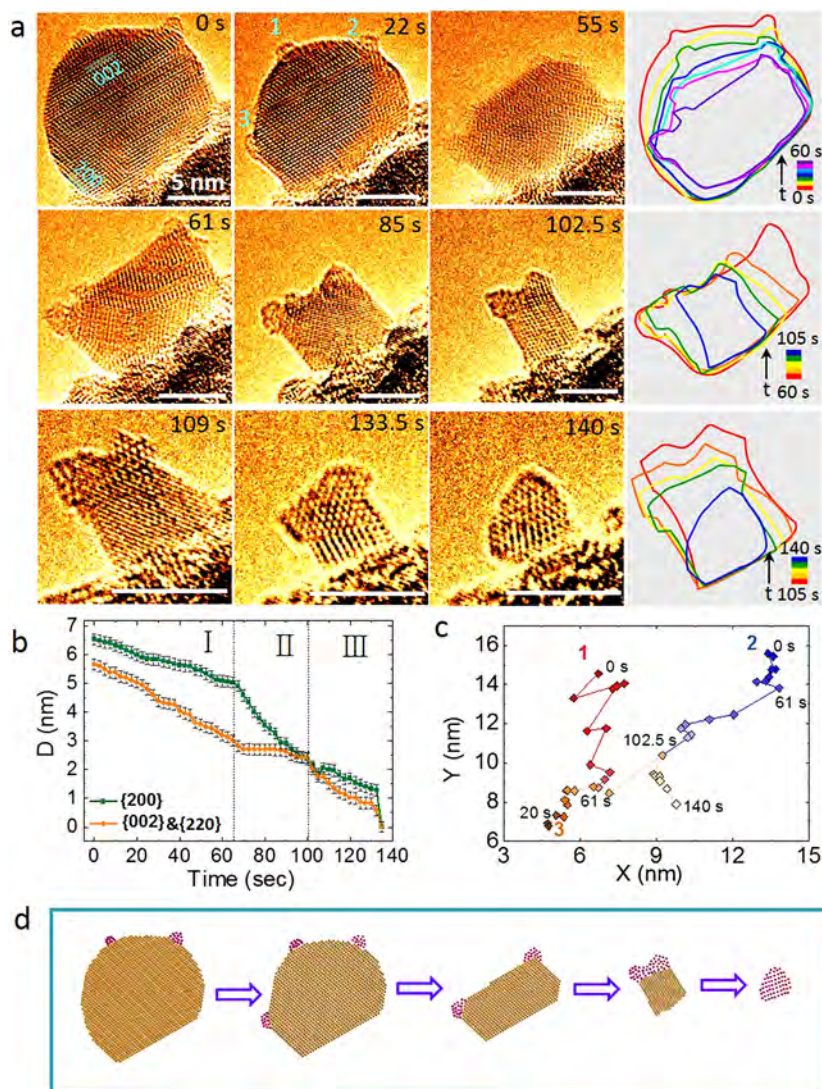


**Figure 2.** Anomalous shape evolution of a  $\text{Ag}_2\text{O}_2$  nanocrystal with Ag surface adsorbates. (a) Sequential HRTEM images (false color) show the real-time shape evolution of the  $\text{Ag}_2\text{O}_2$  nanocrystal with Ag surface adsorbates during etching under an electron beam. Images are extracted from Video S2. The etching process can be divided into three regimes: spherical-to-cuboidal shape transformation, side etching, and bottom etching. The corresponding time-labeled contours in each regime are listed in the right column. The original HRTEM images are shown in Figure S12. (b) The measured average distances from the center of the nanocrystal to (200) and (002) and (220) facets as a function of time. Error bars indicate the standard deviation. (c) Migration trajectories of three surface adsorbates including a newly formed one. (d) Schematic illumination of the anomalous etching process.

show that etching of the nanocrystal occurs mostly in the upper part with the exposed surface. We quantified the evolution of the nanoparticle shape by tracking the propagation of different facets. We first determine the crystal center of the  $\text{Ag}_2\text{O}_2$  particle (Figure S6) and measure the distance from the center of the crystal to these three facets: (002),  $\{\bar{1}11\}$ , and  $\{\bar{1}\bar{1}\bar{1}\}$  (Figure 1b). The distances as a function of time are plotted in Figure 1e. The etching rate of each facet (slope of each plot) is roughly proportional to their surface free energy ( $\{002\} \sim 1.98$  eV per Ag atom,  $\{\bar{1}11\} \sim 1.57$  eV per Ag atom, and  $\{\bar{1}\bar{1}\bar{1}\} \sim 1.86$  eV per Ag atom) as shown in Table 1. This suggests that the etching process is

near-equilibrium, as predicted by the Wulff construction theory. The atomic pathways of etching on the  $\{\bar{1}\bar{1}\bar{1}\}$  facet are shown in Figure 1f. First, some atoms at the atomic steps with fewer neighbors are removed preferentially (0–3 s). Subsequently, atoms in the outmost layer of  $\{\bar{1}\bar{1}\bar{1}\}$  facet are completely removed (4 s). Due to surface diffusion, some atoms (marked by green balls) can be adsorbed at the steps to “heal” the defects. The subsequent etching of the  $\{\bar{1}\bar{1}\bar{1}\}$  facet (Figure S7) and the etching of the  $\{\bar{1}\bar{1}\bar{1}\}$  facet (Figure S8) show similar trends. Therefore, the shape evolution of the  $\text{Ag}_2\text{O}_2$  nanocrystal without surface adsorbates is near-

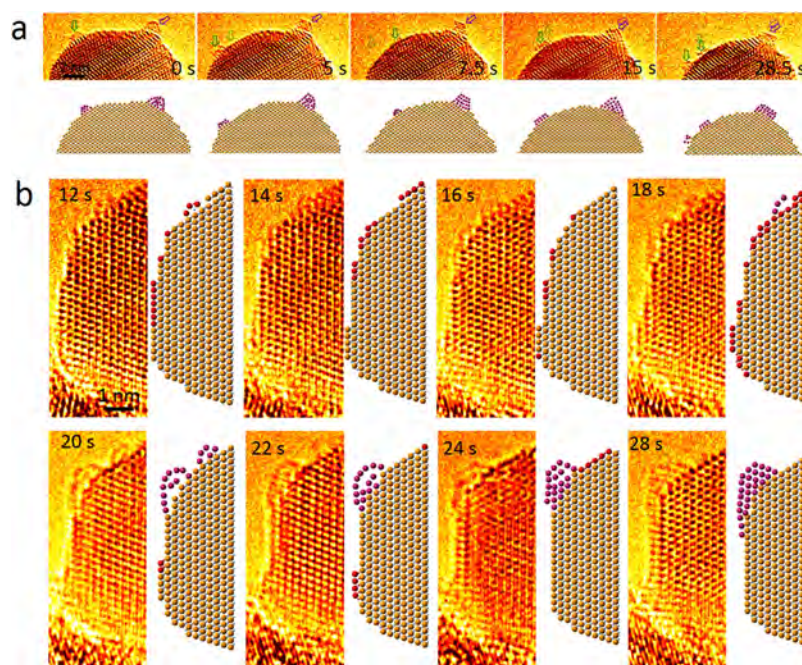


**Figure 3.** Selective capping and dynamics of Ag surface adsorbates on the  $\text{Ag}_2\text{O}_2$  nanocrystal. (a) Sequential HRTEM images (false color) and atomic models show the movement of Ag surface clusters on the  $\text{Ag}_2\text{O}_2$  surface during electron beam etching. The Ag clusters adsorbed at the junction between the (200) and (002) facets terminals (marked by purple arrows) are more stable than those on the (002) facets (marked by green arrows). (b) Sequential snapshots of HRTEM images and atomic models show the in situ growth of an Ag surface adsorbate and its adjustment function during electron beam etching. The corresponding original HRTEM images are shown in Figure S15.

equilibrium-dominated by surface free energy and modified by surface diffusion of adatoms.

Etching of the  $\text{Ag}_2\text{O}_2$  nanocrystal with Ag surface adsorbates is very different from that of the regular  $\text{Ag}_2\text{O}_2$  nanocrystal with a clean surface. For example, a  $\text{Ag}_2\text{O}_2$  nanocrystal with the same monoclinic structure has two adsorbates on the surface of a nanocrystal (Figure S9). Due to the small sizes and the dynamic nature of the clusters, we cannot directly determine the crystal structure of the surface adsorbates during etching. However, through HRTEM and EELS spectra of the remaining cluster, it is clear that the surface adsorbates are Ag clusters with a hexagonal closest packed structure (Figure S11). Figure 2a shows the real-time shape evolution of a  $\text{Ag}_2\text{O}_2$  nanoparticle with Ag surface adsorbates during etching, and the corresponding time-labeled contours are listed in the right column.

Based on the characteristics of the shape changes, the etching process of a  $\text{Ag}_2\text{O}_2$  nanocrystal with the Ag surface adsorbates can be divided into three regimes: spherical-to-cuboidal shape transformation (0–60 s), side etching (60–105 s), and bottom etching (105–140 s). At the initial stage, atoms at the steps with fewer neighbors are sputtered away preferentially, and some atoms diffuse on the surface randomly to heal defects (see Figure S13), which is similar to the etching of the nanoparticle with a clean surface. Subsequently, the etching of the (002) facet becomes faster and the sphere-like nanoparticle transforms to cuboid-like shape (22–60 s) as shown in Figure 2a. During this process, a new Ag cluster marked by the number 3 formed probably due to the reduction of the  $\text{Ag}_2\text{O}_2$  through the formula:  $\text{Ag}_2\text{O}_2 \rightarrow \text{Ag} + \text{O}_2$ . Cluster 2 and cluster 3 remain stationary, while cluster 1 moves randomly, and it eventually merges with the cluster 3 as indicated by the contours and migration trajectories in Figure 2c. In the second regime, the  $\text{Ag}_2\text{O}_2$  cuboid nanocrystal is

pinned by the Ag clusters at the corners. Etching proceeds by gradually removing the side surface, and there is almost no change in the vertical direction (Figure 2b). The method of determining the center of the particle (reference point) in Figure 2a is shown in Figure S14.

The etching is mainly along the right side of the nanocrystal from 61 to 85 s, but both sides are etched after 85 s; this observation will be discussed in more detail later in this Letter. In the end, the three Ag clusters are combined to form a large one. In the last regime, the top of the  $\text{Ag}_2\text{O}_2$  nanocrystal is completely capped with a Ag cluster. Intuitively, with the protection of a Ag cluster, the  $\text{Ag}_2\text{O}_2$  nanocrystal can only be etched from the side. However, as the width decreases, the height also decreases accordingly likely due to minimization of the surface free energy of a certain volume, which is different from the case of the second subprocess (Figure 2b). Eventually, the  $\text{Ag}_2\text{O}_2$  nanocrystal is completely etched away, leaving only the surface adsorbates.

We further find that the etching rate of the (200), (002), and (220) facets is not proportional to their theoretical surface free energy ((200), 2.05 eV per Ag atom; (002), 1.98 eV per Ag atom; (220), 2.23 eV per Ag atom as listed in Table 1). Therefore, etching of the  $\text{Ag}_2\text{O}_2$  nanocrystal with Ag surface adsorbates is characterized by nonequilibrium shape transformation. The shape evolution process is highlighted in Figure 2d.

To further study the microscopic mechanisms behind the anomalous shape evolution of the  $\text{Ag}_2\text{O}_2$  nanocrystal, we focus on the influences of Ag surface clusters on the sphere-to-cuboid transformation. Figure 3a shows the Ag surface adsorbates on the  $\text{Ag}_2\text{O}_2$  nanocrystal surface, while the nanocrystal is etched away. At the initial state, cluster 1 (marked by green arrow) sits on the (002) facet and cluster 2 (marked by purple arrow) is adsorbed at the junction between

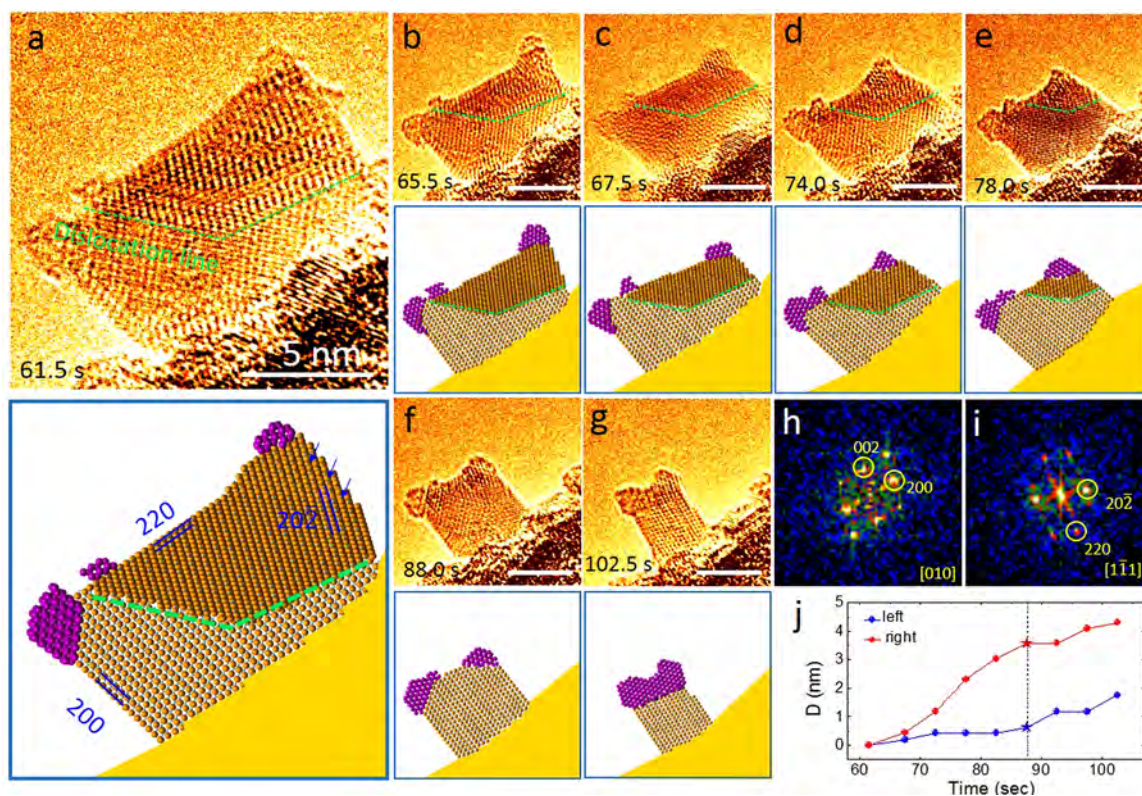


**Figure 4.** Asymmetric side etching of the cuboidal  $\text{Ag}_2\text{O}_2$  nanocrystal with Ag surface adsorbates. (a–g) Sequential HRTEM images (false color) and the atomic models show that the etching speed of the  $\text{Ag}_2\text{O}_2$  nanocrystal is faster on the right side than the left. The atoms of Ag clusters are marked with purple, and the Ag atoms in the  $\text{Ag}_2\text{O}_2$  nanocrystal are marked with orange. The corresponding original HRTEM images are shown in Figure S16. (h, i) Corresponding FFT patterns of bottom part and top part, which are separated by the dislocation line. (j) The measured distances from the center of the nanocrystal to the left and right facets as a function of time.

the (200) and (002) facets. Then, cluster 1 moves randomly on the (200) facet, while the nanocrystal is etched away. It splits into two at 28 s, and the right one quickly combines with cluster 2. Meanwhile, cluster 2 is almost stationary at the facet junction. The behavior of Ag clusters on the  $\text{Ag}_2\text{O}_2$  nanocrystal surface is likely due to the energy variations of different positions. For instance, the Ag cluster is fixed at the corner due to a high adsorption energy, while it moves randomly on the flat (002) surface without a preferable location and eventually bonds with the atoms at the corners of the  $\text{Ag}_2\text{O}_2$  crystal. Figure 3b shows the formation of a new Ag cluster and how it affects the etching of different facets at the atomic level. From 12 to 16 s, etching starts from the atomic steps and some atoms diffuse on the surface to form adsorbed atoms. These atoms come together to form a cluster (see details in frames between 18 and 28 s). Before the cluster formation, two layers of the (200) facet and three layers of the (002) facet are etched (12–22 s). However, after the cluster formation, only the (002) facet is etched. Etching along the (200) facet is stopped, which is probably due to a Ag cluster that caps the atomic steps of the (200) facet. The (002) facet has two terminals, and even though the left terminal is capped with the Ag cluster, etching can still proceed along the atomic steps at the right terminal. Further etching leads to the conversion of a spherical nanocrystal to a cuboid.

As mentioned above, in the second regime of etching, the etching rate on the right side of the cuboidal  $\text{Ag}_2\text{O}_2$  nanocrystal is much faster than that on the left side (61.5–88 s). After 88 s, the etch rates on both sides become similar. Figure 4a shows the  $\text{Ag}_2\text{O}_2$  nanocrystal is divided into two

parts by one dislocation line. The corresponding FFT patterns (Figure 4h,i) of these two parts indicate that they have the same crystal structure but along different zone axes with the bottom along [010] and the top along [111]. As shown in the atomic model in Figure 4a, the (200) facet on the left, (220) facet on the top, and the (202) facet on the right side are highlighted.

We calculate the facet energy of a  $\text{Ag}_2\text{O}_2$  nanocrystal using the density functional theory (DFT), and the results are shown in Table 1. Comparing the surface energy of the (200) facet (2.05 eV per Ag atom) and the (220) facet (2.23 eV per Ag atom), the etching is preferential along the sides of the  $\text{Ag}_2\text{O}_2$  nanocrystal in order to reduce the surface energy. As shown in Figure 4a–e, there are no atomic steps on the left side, while there are some on the right side as pointed out by blue arrows. The atoms at the atomic steps have fewer neighbors, which may be etched away quickly. As the etching progresses, the dislocation line gradually moves to the corner until it disappears at 88 s (Figure 4a–e). At that moment, both sides of the crystal are {200} facets, and the majority of atomic steps disappear (Figure 4f,g), resulting in almost the same etching rates on both sides. Figure 4j shows the distances from the crystal center to the left and right facet surfaces as a function of time. We first built a Cartesian coordinate system for the sequential images (Figure S17). The coordinate origin of Cartesian coordinate system is a characteristic position on the substrate; the  $x$  axis is parallel to the substrate, and the positions on left and right sides are marked by yellow and blue lines, respectively.  $L_x$  and  $R_x$  ( $x = 0, 1, 2, 3, 4, 5, 6, 7, 8$ ) represent the distance from coordinate origin to the left and

right sides, so we can use this feature position as a reference to study the motion on both sides of the nanocrystal.

## CONCLUSION

In summary, we have observed the anomalous shape evolution of  $\text{Ag}_2\text{O}_2$  nanocrystals modulated by the surface adsorbates during the etching process under an electron beam. The Ag surface adsorbates strongly influence the atomic pathways of  $\text{Ag}_2\text{O}_2$  nanocrystal etching. Different from the etching of  $\text{Ag}_2\text{O}_2$  nanocrystals with a clean surface, which show the near-equilibrium shape evolution,  $\text{Ag}_2\text{O}_2$  nanocrystals with Ag surface adsorbates present a distinct facet development during etching. The facets with atomic steps are etched away preferentially. For the facet without atomic steps, the etch rate is dependent on the surface energy. For example, the etching rates of the (200), (002), and (220) facets are sequentially decreased. Ag adsorbates modify the  $\text{Ag}_2\text{O}_2$  nanocrystal surface configuration by selectively capping the junction between two neighboring facets, which prevent the edge atoms from being etched away and block the diffusion path of surface atoms. This work suggests potential strategies for controlling the nonequilibrium shape transformation of nanocrystals with surface adsorbates. The ability to directly observe the dynamic processes of nanocrystals at the atomic scale may assist the study and design of many other nanocrystals with novel and controlled shapes.

## ASSOCIATED CONTENT

### Supporting Information

The Supporting Information is available free of charge on the ACS Publications website at DOI: 10.1021/acs.nanolett.8b04719.

Synthesis of  $\text{AgVO}_3$  nanorods, preparation of  $\text{Ag}_2\text{O}_2$  nanocrystals, materials characterization and TEM observation, density functional theory calculation, elemental characterization of the as-prepared  $\text{AgVO}_3$  nanoribbons, growth route of  $\text{Ag}_2\text{O}_2$  particles on  $\text{Ag}_{(1-x)}\text{VO}_3$  substrates, elemental characterization of the as-prepared  $\text{Ag}_2\text{O}_2$  nanocrystals loaded on the surface of  $\text{AgVO}_3$ , atomic structure of an  $\text{Ag}_2\text{O}_2$  crystal with a clear surface, original HRTEM images of  $\text{Ag}_2\text{O}_2$ , determination of the crystal center, representative HRTEM images illustrating the etching processes of the  $(\bar{1}\bar{1}\bar{1})$ ,  $(\bar{1}\bar{1}1)$ , and (200) facets, atomic structure of an  $\text{Ag}_2\text{O}_2$  crystal with surface adsorbates, shape and structure of Ag clusters changed randomly during the etching process, characterization of the remaining surface Ag cluster after electron beam etching, HRTEM images, sequential images showing the movements of both left and right sides of the nanocrystal, periodic slabs used to model the different surfaces of  $\text{Ag}_2\text{O}_2$  and calculated surface energy per Ag atom of different crystal facets, crystal structure data, and video captions (PDF)

Video S1 (AVI)

Video S2 (AVI)

## AUTHOR INFORMATION

### Corresponding Authors

\*E-mail: slt@seu.edu.cn.

\*E-mail: hmzheng@lbl.gov.

## ORCID

Litao Sun: 0000-0002-2750-5004

Haimei Zheng: 0000-0003-3813-4170

## Author Contributions

The manuscript was written through contributions of all authors. Q.Z., H.Z., and L.S. conceived the project. Q.Z. performed the in situ TEM imaging. G.G. performed the calculations. Q.Z., Y.S., X.P., Y.W., H.D., and L.W. carried out the data analysis. Q.Z., H.Z., and L.S. cowrote the paper with all authors contributing to the discussion and preparation of the manuscript.

## Notes

The authors declare no competing financial interest.

## ACKNOWLEDGMENTS

This work was funded by the U.S. Department of Energy (DOE), Office of Science, Office of Basic Energy Sciences (BES), Materials Sciences and Engineering Division under contract no. DE-AC02-05-CH11231 within the in situ TEM program (KC22ZH). The work at Southeast University was supported by the National Natural Science Foundation of China (51420105003, 11327901, 11525415, and 11674052). Work at the Molecular Foundry was supported by the Office of Science, Office of Basic Energy Sciences, of the U.S. Department of Energy under contract no. DE-AC02-05CH11231. Q.Z. acknowledges funding support from the China Scholarship Council (201606090071) and Scientific Research Foundation of Graduate School of Southeast University (YBPY1708). We thank Chengyu Song for his help with the Tecnai microscope setup.

## ABBREVIATIONS

HRTEM, high-resolution transmission electron microscope; EELS, energy-loss spectroscopy; FFT, fast Fourier transformation; DFT, density functional theory.

## REFERENCES

- (1) Bell, A. T. *Science* **2003**, *299*, 1688–1691.
- (2) Yan, W.; Mahurin, S. M.; Pan, Z.; Overbury, S. H.; Dai, S. *J. Am. Chem. Soc.* **2005**, *127*, 10480–10481.
- (3) Weimann, S.; Kremer, M.; Plotnik, Y.; Lumer, Y.; Nolte, S.; Makris, K.; Segev, M.; Rechtsman, M.; Szameit, A. *Nat. Mater.* **2017**, *16*, 433.
- (4) Zhang, Q.; Yin, K.; Dong, H.; Zhou, Y.; Tan, X.; Yu, K.; Hu, X.; Xu, T.; Zhu, C.; Xia, W.; et al. *Nat. Commun.* **2017**, *8*, 14889.
- (5) Niu, K.; Xu, Y.; Wang, H.; Ye, R.; Xin, H. L.; Lin, F.; Tian, C.; Lum, Y.; Bustillo, K. C.; Doeff, M. M.; et al. *Science advances* **2017**, *3*, No. e1700921.
- (6) Zhang, Q.; Shi, Z.; Yin, K.; Dong, H.; Xu, F.; Peng, X.; Yu, K.; Zhang, H.; Chen, C.-C.; Valov, I.; et al. *Nano Lett.* **2018**, *18*, 5070–5077.
- (7) Xia, W.; Zhang, Q.; Xu, F.; Sun, L. *ACS Appl. Mater. Interfaces* **2016**, *8*, 9170–9177.
- (8) Sun, S.; Yuan, D.; Xu, Y.; Wang, A.; Deng, Z. *ACS Nano* **2016**, *10*, 3648–3657.
- (9) Zhu, F.; Men, L.; Guo, Y.; Zhu, Q.; Bhattacharjee, U.; Goodwin, P. M.; Petrich, J. W.; Smith, E. A.; Vela, J. *ACS Nano* **2015**, *9*, 2948–2959.
- (10) Syrenova, S.; Wadell, C.; Nugroho, F. A.; Gschneidner, T. A.; Fernandez, Y. A. D.; Nalin, G.; Świtek, D.; Westerlund, F.; Antosiewicz, T. J.; Zhdanov, V. P.; et al. *Nat. Mater.* **2015**, *14*, 1236.
- (11) Wang, X.; Swihart, M. T. *Chem. Mater.* **2015**, *27*, 1786–1791.
- (12) Poul, L.; Hansen, J. B. W.; Helveg, S.; Rostrup-Nielsen, J. R.; Clausen, B. S.; Topsøe, H. *Science* **2002**, *295*, 2053–2055.

- (13) Ringe, E.; Van Duyne, R.; Marks, L. *Nano Lett.* **2011**, *11*, 3399–3403.
- (14) Wulff, G. Z. *Kristallogr. - Cryst. Mater.* **1901**, *34*, 449–530.
- (15) Chen, M.; Wu, B.; Yang, J.; Zheng, N. *Adv. Mater.* **2012**, *24*, 862–879.
- (16) Laibinis, P. E.; Whitesides, G. M.; Allara, D. L.; Tao, Y. T.; Parikh, A. N.; Nuzzo, R. G. *J. Am. Chem. Soc.* **1991**, *113*, 7152–7167.
- (17) Song, H.; Kim, F.; Connor, S.; Somorjai, G. A.; Yang, P. *J. Phys. Chem. B* **2005**, *109*, 188–193.
- (18) Xiong, Y.; Cai, H.; Wiley, B. J.; Wang, J.; Kim, M. J.; Xia, Y. *J. Am. Chem. Soc.* **2007**, *129*, 3665–3675.
- (19) Huang, X.; Zhang, H.; Guo, C.; Zhou, Z.; Zheng, N. *Angew. Chem., Int. Ed.* **2009**, *48*, 4808–4812.
- (20) Liao, H.-G.; Zhrebetskyy, D.; Xin, H.; Czarnik, C.; Ercius, P.; Elmlund, H.; Pan, M.; Wang, L.-W.; Zheng, H. *Science* **2014**, *345*, 916–919.
- (21) Ye, X.; Jones, M. R.; Frechette, L. B.; Chen, Q.; Powers, A. S.; Ercius, P.; Dunn, G.; Rotskoff, G. M.; Nguyen, S. C.; Adiga, V. P.; et al. *Science* **2016**, *354*, 874–877.
- (22) Storm, A.; Chen, J.; Ling, X.; Zandbergen, H.; Dekker, C. *Nat. Mater.* **2003**, *2*, 537.
- (23) Zandbergen, H. W.; van Duuren, R. J.; Alkemade, P. F.; Lientschnig, G.; Vasquez, O.; Dekker, C.; Tichelaar, F. D. *Nano Lett.* **2005**, *5*, 549–553.
- (24) Fischbein, M. D.; Drndić, M. *Nano Lett.* **2007**, *7*, 1329–1337.
- (25) Yu, K.; Zhao, W.; Wu, X.; Zhuang, J.; Hu, X.; Zhang, Q.; Sun, J.; Xu, T.; Chai, Y.; Ding, F.; et al. *Nano Res.* **2018**, *11*, 1–12.
- (26) Lin, J.; Cretu, O.; Zhou, W.; Suenaga, K.; Prasai, D.; Bolotin, K. I.; Cuong, N. T.; Otani, M.; Okada, S.; Lupini, A. R.; et al. *Nanotechnol.* **2014**, *9*, 436.
- (27) Liu, X.; Xu, T.; Wu, X.; Zhang, Z.; Yu, J.; Qiu, H.; Hong, J.-H.; Jin, C.-H.; Li, J.-X.; Wang, X.-R.; et al. *Nat. Commun.* **2013**, *4*, 1776.
- (28) Shen, Y.; Xu, T.; Tan, X.; Sun, J.; He, L.; Yin, K.; Zhou, Y.; Banhart, F.; Sun, L. *Nano Lett.* **2017**, *17*, 5119–5125.
- (29) Tudela, D. *J. Chem. Educ.* **2008**, *85*, 863.
- (30) Sang, Y.; Kuai, L.; Chen, C.; Fang, Z.; Geng, B. *ACS Appl. Mater. Interfaces* **2014**, *6*, 5061–8.